Material state changes as a basis for prognosis in aeronautical structures

K. L. Reifsnider **P. Fazzino** **P. K. Majumdar**
reifsnid@cec.sc.edu **majumdap@cec.sc.edu**
Department of Mechanical Engineering
University of South Carolina
Columbia, South Carolina
USA

L. Xing
Edison International
Boston, Massachusetts
USA

ABSTRACT

The long-term performance of aeronautical structures is typically discussed in terms of concepts such as structural integrity, durability, damage tolerance, fracture toughness, etc. These familiar concepts are usually addressed by considering balance equations, crack growth relationships, and constitutive equations with constant material properties, and constant or cyclically applied load conditions. Loading histories are represented by changing stress (or strain) states, only. But for many situations, especially associated with high performance aircraft, the local state of the material may also change during service, so that the properties used in those equations are functions of time and history of applied conditions. For example, local values of stiffness, strength, and conductivity are altered by material degradation to create 'property fields' that replace the global constants, and introduce time and history into the governing equations. The present paper will examine a small set of such problems and offer a construct for using related solutions to estimate future performance based on history of use and current material state, a concept typically called prognosis.

1.0 INTRODUCTION

Prognosis is the general pursuit of predicting future performance on the basis of current assessment and history of behaviour. The traditional concept of prognosis is most familiar in the context of medical evaluation of the condition and prospects of a patient. For structural mechanics, there is an array of contexts and interpretation. One such scenario is the prediction of the stability or likelihood of collapse from information about response to 'safe' loading conditions[1,2]. Another context has to do with the large context of health monitoring, in which structural characteristics such as stiffness[3], or more localised information from either passive (e.g. acoustic emission) or active (e.g. surface wave excitation response)[4,5] assessment is used to evaluate 'degradation' as a method of estimating future performance. A rather robust literature presents a context of fracture mechanics, focused on localised deformation, crack initiation and propagation, in some cases including specific address of the effects of local constituent particle effects on that sequence on prognosis of performance and life[6]. And finally, there are contexts based on crystal plasticity in which, for example, microstructure characterisations are used to anticipate the relationship between shear strain and damage nucleation on a local scale, e.g., at grain boundaries[7].

The focus of the present paper is very different. We are concerned with heterogeneous materials which have meso-phases that are very brittle, e.g., woven fibre reinforced polymer composites. The paper addresses large (nonlinear) strains in such materials, which appears, at first glance, to be a contradiction. But under at least three conditions of practical interest, large nonlinear strains occur in such materials, and are responsible for important performance characteristics:

1. In the materials considered for structural design-levels of stress and strain for long-term service, the accumulation of damage is large before 'failure' occurs, and greatest of all cases typically

Paper No. 3405. Manuscript received 11 February 2009, accepted 21 July 2009.

https://doi.org/10.1017/S0001924000003444 Published online by Cambridge University Press

considered since long-term accumulation at low stresses maximises degradation under mechanical loading before performance drops below the acceptable (design) levels (i.e., longest time and lowest stress equals most damage-induced strain before failure).

2. Out of plane loading, for which large displacements and highly nonlinear stress states can create large local strains.
3. High-rate loading for which energy dissipation by shear-strain nonlinearity can be a critical mechanism that contributes to impact resistance and damage tolerance.

We will approach these requirements by establishing constitutive relationships for highly nonlinear strains (up to 20%) in woven-fibre reinforced polymer composites as a foundation for understanding stiffness and strength changes in anisotropic materials as state changes associated with distributed micro-cracking in uniform stress states.

For such materials, and for large strain and long term loading conditions, prognosis requires that we follow the mechanisms and extent of extensive damage accumulation. For this purpose, we have selected out-of-plane bending of thin structural composites as a method of introducing non-uniform distributions of damage. In this paper we introduce a new method of following the induced material state changes, based on multi-physics formulations. Specifically, we use electrochemical impedance spectroscopy to follow and understand conductivity changes as a second material property that varies with changes of state.

With this new methodology in hand, we address the question of how to predict future performance based on understandings of material state changes induced by prior service. We will offer suggested directions and observations in that section, but this part of the effort is work in progress.

2.0 NONLINEAR RESPONSE OF 'BRITTLE' MATERIALS: CONSTITUTIVE EQUATIONS

Continuous-fibre reinforced structural composite materials are typically classified as 'brittle' with strain to break in the principal fibre directions of only a few percent or less. However, fibre architectures and material choices can provide 'ductility' that is highly dependent on microstructure. In some situations, the off-axis 'ductility' of woven fibre architectures can be exploited to greatly improve performance. One of those situations is blast loading, in which out-of-plane, high-rate loading is applied over a fairly localised area. The structural analysis of this kind of material behaviour is dependent on the construction of constitutive models that can collectively represent the large deformation, rate dependent and temperature effects correctly.

Constitutive models for anisotropic materials like structural composites which include strain rate effects have been discussed by several authors[8-15]. That research shows that a constitutive model for characterising strain rate dependency can be developed based on experimental data. However, most models have only been able to represent the material response up to about four percent strain to break. The need to represent progressive failure up to (and including) rupture strains of the order of 20% as a basis for structure analysis (especially with commercial codes) is a driver for the present research.

2.1 Overview of the constitutive formulation for in-plane loading

In this element of our study, a plain-weave vinyl ester material was selected and a number of different strain rates and temperatures were used in tensile tests of off-axis coupon specimens. A generalised three-parameter constitutive model is first discussed to model the large deformation stress-strain relationship. Then a new micromechanical model based on woven composite microstructure analysis is presented that represents the material behavior up to the rupture strain. The proposed constitutive model was used to predict the material response at different strain rates and temperature. The model predictions were verified by a different set of tests. The basic concepts and methodology involved in reducing such data to constitutive equations that can be used in commercial computational codes such as ABAQUS™ to enable structural analysis in the presence of large strain progressive damage under multi-axial dynamic loading are discussed in this section. Parts of this work have been published earlier[14,15], so we will summarise only the information needed for the present discussion, below.

If we consider two-dimensional stress states in an orthotropic material, we require the engineering constants, $E_1, E_2, G_{12}, \frac{\nu_{12}}{E_1} = \frac{\nu_{21}}{E_2}$.

Then the elastic potential may be written as

$$w = \frac{1}{2}\left(\frac{\sigma_{11}^2}{E_1} - \frac{2\nu_{12}}{E_1}\sigma_{11}\sigma_{22} + \frac{\sigma_{22}^2}{E_2} + \frac{\sigma_{12}^2}{G_{12}}\right) \quad \ldots (1)$$

If uniaxial loading is applied by stress σ_θ at an angle θ to the material axis of symmetry (fibre directions), the potential w becomes

$$w = \frac{1}{2}\sigma_\theta^2\left(\frac{1}{E_1}\mathrm{Cos}^4\theta + \left(\frac{1}{G_{12}} - \frac{2\nu_{12}}{E_1}\right)\mathrm{Sin}^2\theta\,\mathrm{Cos}^2\theta + \frac{1}{E_2}\mathrm{Sin}^4\theta\right) \quad \because . (2)$$

The linear strain ε_θ is expressed as $\varepsilon_\theta^l = \frac{\partial w}{\partial \sigma_\theta} = \frac{\sigma_\theta}{E_1}h_l^2(\theta)$ where $h_l^2(\theta) = \mathrm{Cos}^4\theta + c_1\mathrm{Sin}^4\theta + c_2\mathrm{Sin}^2\theta\,\mathrm{Cos}^2\theta$ The constants $c_1 = \frac{E_1}{E_2}, c_2 = \frac{E_1}{G_{12}} - 2\nu_{12}$ reflect the ratio of elastic and shear moduli. Introducing new variables $\tilde{\varepsilon}_\theta^l = \frac{\varepsilon_\theta^l}{h_l(\theta)}$ and $\tilde{\sigma} = \sigma_\theta h_l(\theta)$, the stress-strain relationship becomes angle independent, i.e., $\tilde{\varepsilon}_\theta^l = \frac{1}{E_1}\tilde{\sigma}_\theta; \tilde{\varepsilon}_\theta^l / \tilde{\sigma}_\theta = \mathrm{const.}$

If only off-axis tensile tests are used, the constants c_1 and c_2 can be uniquely determined from the best fit of Equation (2) for all test angles. For nonlinear deformation, Ogihara and Reifsnider[8] have introduced a three parameter generalisation of the 2D single-constant plasticity model originated by Sun and Chen[11] to construct a constitutive representation of the nonlinear quasi-static behaviour of angle-ply laminates. A quadratic yield function is assumed for the 3D composite in the form:

$$\begin{aligned} 2f(\sigma_{ij}) &= a_{11}\sigma_{11}^2 + a_{22}\sigma_{22}^2 + a_{33}\sigma_{33}^2 + 2a_{12}\sigma_{11}\sigma_{22} \\ &+2a_{13}\sigma_{11}\sigma_{33} + 2a_{23}\sigma_{22}\sigma_{33} + 2a_{12}\sigma_{11}\sigma_{22} + 2a_{44}\sigma_{23}^2 \\ &+2a_{55}\sigma_{13}^2 + 2a_{64}\sigma_{12}^2 = k \end{aligned} \quad \ldots (3)$$

where k is a state variable and the stresses are referred to the principal material directions. The yield function is taken as the plastic potential function from which the incremental plastic strain can be derived in the usual way. Introducing an effective stress, $\sigma^* = \sqrt{3f}$ one can write and $dW^p = \sigma_{ij}d\varepsilon_{ij}^p = 2fd\lambda = \sigma^* d\varepsilon^{*p} \Rightarrow d\varepsilon^{*p}$

$$= \frac{2}{3}\sigma^* d\lambda \text{ and } d\lambda = \frac{3}{2}\left(\frac{d\varepsilon^{*p}}{d\sigma^*}\right)\left(\frac{d\sigma^*}{\sigma^*}\right) \quad \ldots (4)$$

where ε^{*p} is the effective plastic strain and W^p is the plastic work per unit volume. The plastic slope, $\left(\frac{d\varepsilon^{*p}}{d\sigma^*}\right)$ is generally rate dependent. For plane stress Equation (3) reduces to four terms. For unidirectional loading, σ_x, in a direction that forms a positive angle θ with

https://doi.org/10.1017/S0001924000003444 Published online by Cambridge University Press

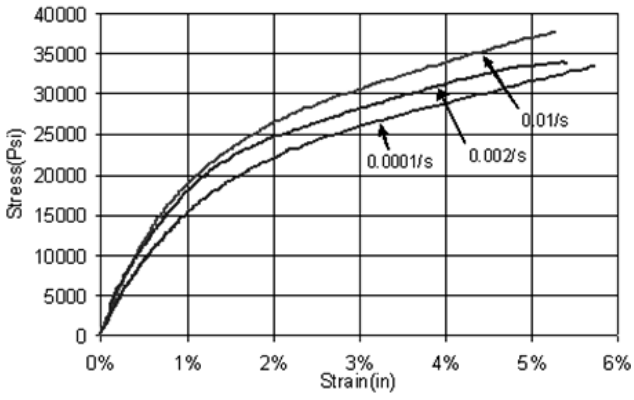


Figure 1. Tensile behaviour for specimens loaded at different strain rate at 15º to the principal material direction.

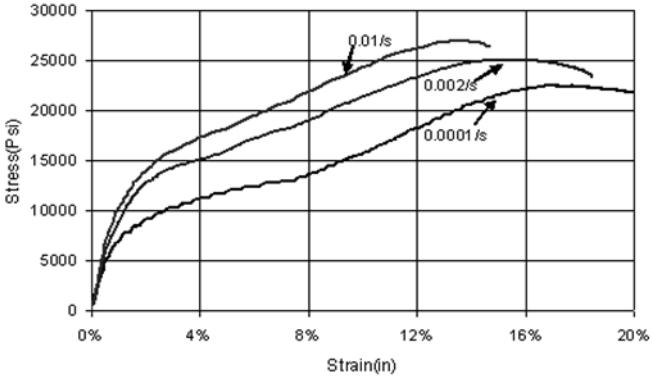


Figure 2. Tensile behaviour for specimens loaded at different strain rate at 45º to the principal material direction.

the fibre direction, x_1 , the stress components in the material system are

$$\sigma_{11} = \sigma_x \mathrm{Cos}^2(\theta) \quad \sigma_{22} = \sigma_x \mathrm{Sin}^2(\theta) \quad \sigma_{12} = -\sigma_x \mathrm{Sin}(\theta)\,\mathrm{Cos}(\theta) \qquad \ldots (5)$$

Whereupon $\sigma^* = \sigma_x h(\theta)$ and

$$\sigma_{11} = \sigma_x \mathrm{Cos}^2(\theta) \quad \sigma_{22} = \sigma_x \mathrm{Sin}^2(\theta) \quad \sigma_{12} = -\sigma_x \mathrm{Sin}(\theta)\,\mathrm{Cos}(\theta) \qquad \ldots (6)$$

For woven composites, Ogihara proposed that $a_{11} = 1$, resulting in the most general three parameter plasticity model for planar problems and uniaxial loading[9] . Then the plastic potential function reduces to

$$2f = \sigma_x^2 h^2(\theta) \text{ with } h(\theta) = \sqrt{\frac{3}{2}\left(\mathrm{Cos}^4\theta + a_{22}\,\mathrm{Sin}^4\theta + 2(a_{12}+a_{66})\mathrm{Sin}^2\theta\,\mathrm{Cos}^2\theta\right)} \qquad \ldots (7)$$

Since the effective stress-strain relation should be a material property under monotonic loading, the material parameters in Equation (7) must be chosen so that the $\sigma^*(\varepsilon^{*p})$ relations are independent of loading angle. If Equation (7) is cast in the following form, it is possible to determine c_1 and c_2 in the following manner.

$$h(\theta) = \sqrt{\frac{3}{2}\mathrm{Cos}^4\theta + c_1\mathrm{Sin}^4\theta + 2c_2\mathrm{Sin}^2\theta\mathrm{Cos}^2\theta} \qquad \ldots (8)$$

We can determine the parameters of the plastic potential function so that the effective-stress, $\sigma_x \cdot h(\theta)$ *vs* the nonlinear effective-strain, $\varepsilon^n/h(\theta)$, forms a single master curve. It is seen that for $\theta = 90^o$,$h(90^o)$ depends only on the potential function parameter c_1. Hence, for our plain weave material, we can determine the numerical value of c_1 from the test data of the fibre principle directions (0º, and 90º) specimens. Having obtained c_1, we can determine the parameter c_2 so that the effective stress-effective strain data for other θ values converge into one single curve to form a master curve for the nonlinear response. To validate these concepts, tensile tests were performed at various strain rates from low (0·0001/s) to moderate (0·01/s) and at different temperatures on an InstronTM servo-hydraulic testing machine. The basic results have been reported earlier, and will only be summarised here[14-15].

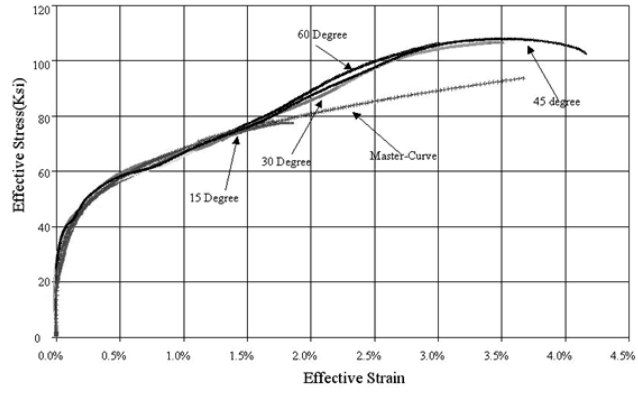


Figure 3. Master curve of effective stress-effective plastic strain for 0·002/s off-axis tension test with C_1 = 0·98, C_2 = 20.

Figures 1 and 2 show test results for two specimen angles (15º and 45º) at different strain rates. Those data show that strain rate dependence is evident in such materials, even for strain rates that differ by only a few orders of magnitude. The largest strain to failure occurs for the 45° orientation in these materials for which strains to break of the order of 20% are observed.

We can determine the parameters of the plastic potential function so that the effective-stress, $\sigma \cdot h(\theta)$ *Vs* nonlinear effective-strain $\varepsilon^n/h(\theta)$, forms a single master curve, as shown below in Fig. 3 for the data in Figs 1 and 2

From our test data, as shown in Figs 1 and 2, we obtained c_1 = 0·98, c_2 = 20 for all strain rates considered. We formulated the master effective stress-effective strain curve by fitting the data by a power law as

$$\bar{\varepsilon}^p = \varepsilon^{*p} = A\left(\bar{\sigma}\right)^n = A(\sigma^*) \qquad \ldots (9)$$

in which, amplitude A is a function of strain rate as

$$A = \chi\left(\dot{\bar{\varepsilon}}^p\right)^m \qquad \ldots (10)$$

and where χ and m are constant.

We were able to make n converge to a single value for different strain rates. However, the A values showed a strong strain rate dependence. Having a set of different values of A, we were able to calculate χ and m values based on logarithmic transformations; then we used linear extrapolation to get different A values at different strain rates.

Figure 4 shows an example of the predicted response compared to observed for one strain rate and angle of loading; results for all other cases are comparable. The general engineering response of the anisotropic material is recovered, including the load-strain point of failure. The representation does not match the response well above 10% strain in some cases, since a simple power law was used here. Other choices for the parametric form of the plastic stress/strain curve are possible (and were confirmed) but involve more complexity which may not be justified and is not necessary for the present discussion.

https://doi.org/10.1017/S0001924000003444 Published online by Cambridge University Press

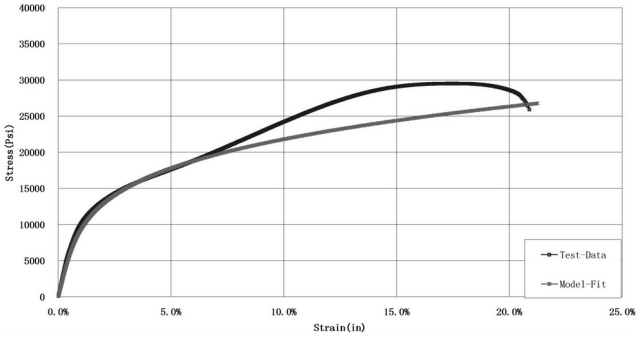


Figure 4. 45° off-axis single curve model at 0·01/s strain rate.

Table 1
Material constant C_θ for different strain rates and orientations

Strain rate	Orientation (degree)	$h(\theta)$	t_b	$t_\theta = t_b h(\theta)^n$ (n = –0·8)	$C_\theta = t_\theta\,(\dot{\varepsilon})^m$ (m = 0·998)
0·0001	15	2·250	999	522·17909	0·0522
	30	3·490	1,632	600·42645	0·0600
	45	3·966	2,088	591·20464	0·0591
	60	3·490	1,660	610·72788	0·0611
	90	1·222	836	712·63169	0·07123
0·002	0	1·225	35·5	30·18505	0·0604
	15	2·250	56·4	29·48038	0·0590
	30	3·490	89	32·74384	0·0655
	45	3·966	101·4	33·67874	0·0674
	60	3·484	83·2	30·65214	0·0613
	90	1·222	42	35·7184	0·0716
0·01	0	1·225	7·8	6·63221	0·0663
	15	2·250	10·63	5·55632	0·0556
	30	3·490	16·5	6·07049	0·0607
	60	3·490	15·3	5·62900	0·0563
	90	1·222	9·2	7·83845	0·0738

2.2 Incorporating the effect of strain rate in anisotropic materials

The question of constructing an engineering failure criterion which embraces strain rate and anisotropy was also addressed. Following the concept of Monkman-Grant[16] expressions of the following form were introduced. The classical form

$$t_b \cdot \left(\dot{\varepsilon}\right)^m = C_1 \text{ recast as } C_\theta = t_\theta \cdot \left(\dot{\varepsilon}\right)^m \qquad \ldots (11)$$

where time to break is t_b, C_1 and C_θ are material constants, and the exponent m is also a material constant that turns out to be very close to unit value. Table 1 below shows the time to failure data for different ply orientations and strain rates reduced by these formulae, with the new variable t_θ defined as the product of the time to break, t_b and the nth power of the orientation function $h(\theta)$ which is the expression introduced earlier. The value of the material constant, n, used in the present case is also shown in Table 1.

The remarkable result of this interpretation is the premise that C_θ is a universal material constant for all of the represented conditions, i.e. it is a single material constant that represents the strength of the anisotropic material in all directions of loading, for strain rates over two orders of magnitude.

This result suggests that there is a single material property that controls fracture for all angles of loading, and looking at the dimensional details of Equation (11), strain to break in a principle material direction is a candidate for that material constant. To examine that premise, we postulate a mechanistic process for the elastic and 'plastic' strain in our materials.

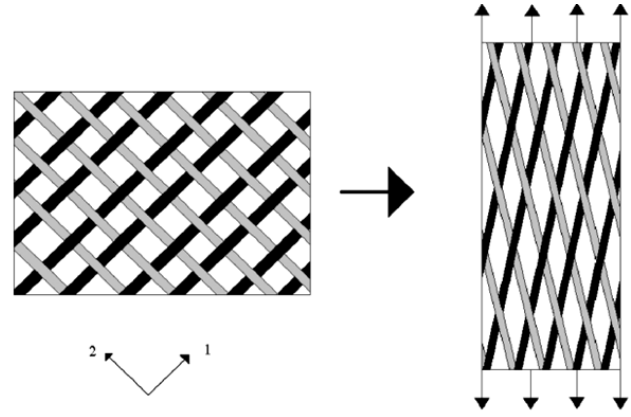


Figure 5. Trellis Shearing deformation of plain weave composite material.

2.3 Estimating the strain-to-break

For off-axis tensile loading after the initial elastic range (<0·5%) the matrix begins to crack and unloads the local stress to the fibres; we represent this process by changing the shear modulus, G_{12}, as suggested by a number of investigators[13]. We can use this damage mechanism to calculate the total strain based on the classical laminate theory using the experimental determination of changes in shear modulus, G_{12}. Using classical laminate theory, after matrix cracking, the new value of G_{12} was considered to be a new material property representing the reduction in the shear deformation resistance. Based on the new G_{12} value one can calculate the new elastic strain that includes the plastic strain caused by matrix cracking.

For loading angles less than 15° away from the warp or weft directions, fracture is clearly a fibre dominated property; the composite fails due to fibre rupture in the warp or weft direction. For specimen angles larger than 15°, the fracture is more strongly influenced by shear deformation, i.e. the limiting shear stress or strain is exceeded. For the plastic strain model, it is obvious that the off-axis large strain to failure of the woven composite is closely associated with its internal fibre geometry characteristics. A distortion of the off-axis plain coupon specimens results in a change in fibre orientation. The in-plane reinforcing fibres inclined by a smaller angle to loading direction have a tendency to rotate to be aligned with the loading axis. The effect of relative rotation of a lamina in the woven composite is significant, and the magnitude has no noticeable strain rate dependency. It was found that the change in angles for different fibre orientations was almost the same (about 5° in these materials) for all angles-of-loading. This may be due to the fact that the cracked matrix in each yarn still occupies a certain amount of volume that resists the further rotation of the fibres, and it may also be associated with 'locking' of the woven fibres in contact with each other.

If we simplify the complex structure of the woven fabric composite during the damage procedure, we may calculate the shear deformation using the geometric concept known as trellis shearing as shown in Fig. 5, and then add the linear elastic tension strain provided by classical laminate theory in order to estimate the final strain to failure of a specimen for off-axis loading. Here we assume that the warp and weft fibre can twist in a pure shearing deformation and that additional matrix crack residuals do not affect the deformation path. Based on the above idealisation, we can estimate strain to failure for any specimen orientation angle that is needed to characterise the material mechanical properties in support of structural analysis.

As discussed above, the large deformation of this woven fabric composite has been simplified to the combination of elastic strain ε_E and trellis shearing deformation ε_m, and the composite structure was represented as a sum of representative unit cells (Fig. 5) as suggested by prior research[14]. Results of these estimates are shown in Table 2.

https://doi.org/10.1017/S0001924000003444 Published online by Cambridge University Press

Table 2
Comparison of strain to failure data of different fibre orientations

	15°	30°	45°
Elastic strain under changed G_{12}	3·81%	7·64%	8·51%
Plastic strain due to fibre shearing	1·95%	4·65%	8·34%
Total strain to break — calculated	5·76%	12·29%	16·85%
Total strain to break — observed	5·35%	15·1%	19·8%

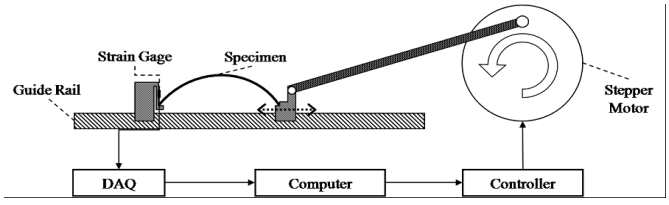


Figure 6. End-loaded bending test setup for cyclic loading of composite coupon.

Subsequent to these estimations, Huffner (a co-investigator in related work) has shown that a simple finite strain definition of failure based on the fully nonlinear deformation gradients in the form of the Green-Lagrange strain tensor captures all of the physical behavior noted above, and confirms that the fibre strain to break (properly determined) controls the final fracture in off axis specimens[17].

2.4 Summary of the constitutive formulation effort

So we have achieved the first objective of our paper, to construct a constitutive approach that includes large-strain progressive damage, up to and including the strain to break. Strain to break was predicted for general off-axis loading from limited pilot observations of deformation and failure modes, and simple micromechanical concepts. A single material parameter was defined which was able to estimate material strength in all loading directions and at all strain rates for the material tested. The resulting analysis is robust and complete, and forms an excellent constitutive platform for implementation in commercial codes for structural analysis of composite structures subjected to high-rate loading.

2.5 The novel path towards prognosis

For prognosis, we need two additional features. The first is an experimental method for following the details of the process we have represented with a nonlinear constitutive law, i.e., to associate a specific material state with specific points on the (master) stress-strain curve, and the second is to follow this association during long-term loading histories of such materials in aeronautical structures. For this purpose, we introduce a new experimental methodology and multi-physics philosophy based on the conductivity of these materials when subjected to low-voltage alternating current, a classical concept called electrochemical impedance spectroscopy (EIS).

3.0 NEW CONCEPT OF MATERIAL STATE CHANGES DURING LONG-TERM CYCLIC LOADING

For this element of our study, end-loaded bending of coupons of woven-glass reinforced polymer composite specimens was used to induce non-uniform local damage accumulation under out-of-plane deformation conditions. This brings us closer to the prognosis of structures under practical engineering conditions. Figure 6 shows an illustration of the cyclic bending experiment.

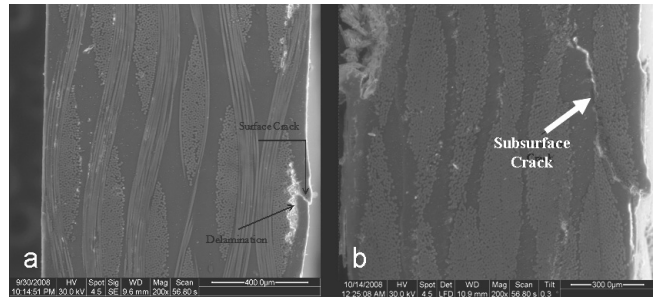


Figure 7. Damage initiation under cyclic end-loaded bending in woven-glass reinforced polymer composites. Tension side is on the right of each photograph. Loading is in the principal fibre direction for (a), in an off-axis for case (b).

Woven-glass reinforced polymer composite specimens were used to develop a data set of fatigue results, including examinations of material state changes (especially matrix cracking) as a function of loading angle (relative to the material principal axis), and residual strength under tensile loading (c.f., Fazzino[18]). Norplex-Micarta Inc. provided NP130 E-glass, plain weave thin laminated composite plates with a halogenated epoxy resin matrix for the experimental work. The fibre volume fraction was 55%. Total specimen thickness (for the five ply laminates used) was about 1mm.

In order to try to make direct associations between the global loading histories and data, and the local material state changes associated with the damage that accumulated during the cyclic loading, we have adapted the method of electrochemical impedance spectroscopy (EIS) to the task of following the local details of damage development and accumulation. Details of the experimental methods developed for this purpose can be found in Ref. 18. For our purposes, we only need to examine how the results can be applied to the current objective.

3.1 Novel concept of identifying conduction path with damage accumulation

For the end-loaded conditions shown in Fig. 6, the stress and strain along the length of the specimen is non-uniform, with a maximum in the middle of the span where the curvature is greatest. This feature provided a gradient of damage under cyclic loading as a function of position along the specimen, and provided a structural detail that is similar to the nonlinear conditions found in joints and geometric features in aeronautical structures. In the present study, bending amplitudes were selected to induce specimen failure under cyclic loading for lives of a few thousand up to about 100,000 cycles. For the woven-glass reinforced polymer material used in these tests, under this repeated bending loading, the early damage began near the mid-span tension and compression surfaces, and progressed into the interior of the specimens. Examples of observed damage (through the thickness) are shown in Fig. 7.

As one would expect, damage begins with matrix cracking, which has limited extent in the case of loading along fibre directions (as shown in Fig. 7(a)), but is more extensive for loading along directions of 30-45° from the fibre direction (as shown in Fig. 7(b)). Matrix cracking begins on the tensile side, as expected, and the pattern of matrix cracking is closely associated with tow geometry of the fibre weave pattern. Fracture of the specimen occurs when the damage propagates through the thickness of the specimens to create a continuous fracture path that crosses the fibres. This general process is the subject of much literature (c.f., Reifsnider and Case[13]).

But prognosis requires more than general knowledge. It requires specific knowledge of damage in a specific structure so that future performance of that specific structure can be estimated. And in order to make that estimate, it requires that the nature of that damage, i.e.,

https://doi.org/10.1017/S0001924000003444 Published online by Cambridge University Press

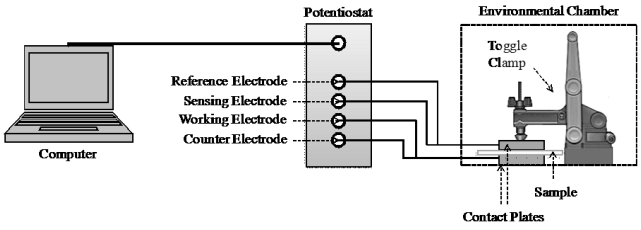


Figure 8. Electrochemical impedance spectroscopy method of examining progressive damage development in cyclically end-loaded composite coupons[19].

the specific details of the changes in material state and local stress state, be determined so that the remaining stiffness, strength and life can be quantitatively estimated for projected loading histories, based on current measurements of the material condition.

To achieve those objectives, we have taken a multiphysics approach. We reasoned that the process of creation of a fracture path in this insulating heterogeneous material is similar in many fundamental ways to the process of creating conduction paths (due to moisture infiltration during damage development) under the excitation of an alternating current. Moreover, the robust nature of the information obtained from such excitation may provide many paths of interpretation of the exact nature of the damage that causes the changes, which enable us to estimate remaining performance.

3.2 Impedance measurement (EIS) to capture material state changes

To test this premise, we adapted an electrochemical impedance spectroscopy (EIS) method, similar to techniques widely used to examine conductivity and electrochemical activity in fuel cells, corrosion conditions, and surface coatings[20]. The general method of introducing an alternating current (AC) signal with cycle frequencies varying from a few hundred to megahertz, across the thickness of the coupon specimens, is sketched in Fig. 8.

The environmental chamber was used to precisely control the level of moisture in the ambient air, which was available to permeate the damaged specimens to create conduction paths as damage developed. Levels of ambient moisture and the presence of conductive ions (e.g., salt solutions) were studied and some multiphysics modelling of the moisture ingress was used to determine the best operating conditions[18].

An example of the output of the method is shown in Fig. 9. In that figure, the real and imaginary parts of the complex resistance (impedance) of the specimen as a function of electrical excitation frequency are plotted, for cyclic loading cycles that correspond to several fractions of life (from a single cycle to the end of life). The real part of the impedance, the Ohmic resistance, is plotted on the abscissa, and the imaginary part (associated with capacitive and inductive impedance) is plotted on the ordinate. Such plot is commonly known as the 'Nyquist plot'. Low frequencies of excitation (1kHz in this case) produce data to the right of the figure, and high excitations (up to 10kHz in this case) produce the data on the left hand side of the figure.

The data curves represent data collected before any loading (top curve), and EIS data collected after 1,000, 2,000, 3,000, 4,000, 5,000 and 6,000 cycles of bending (the specimen fractured at about 7,000 cycles of loading). The orientation of loading for these tests was along one of the fibre directions of the plain weave specimen, so matrix damage before fracture was least of all situations considered. Three tests were conducted for each loading condition; variations in magnitudes of the impedance values from test to test were large in some cases, but relative variations were remarkably small for a given angle of loading, i.e., the results of relative changes were very reproducible. Also, EIS measurements were taken over a 2in length at the mid-span of the specimens and details can be found in Refs 18, 19 and 21.

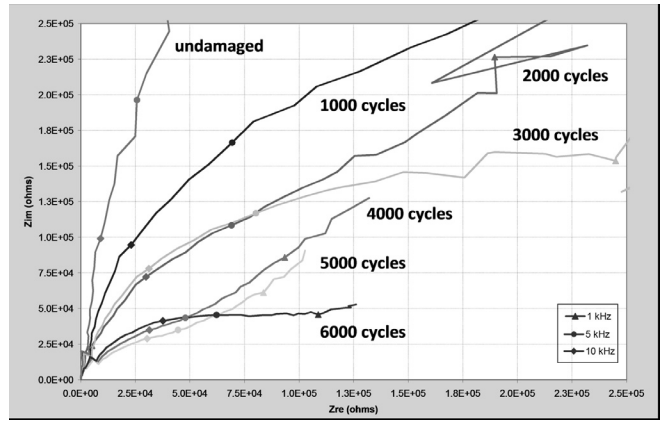


Figure 9. Real and imaginary parts of the electrochemical impedance measured after cyclic loading to several different fractions of life, as a function of frequency of AC excitation. (Colours represent progressive numbers of loading cycles[19]).

Numerous other results are presented in the thesis by Fazzino[18]. However, for the present development, several aspects of this new approach are striking.

3.3 Sensitivity of EIS

The most important of these is almost certainly the remarkable sensitivity of the method to damage development. The greatest difference in the data shown in Fig. 9 is between the results for the undamaged specimen and the results for the specimen cycled to only one thousand cycles, the first 14% or so of the life. And this is for a specimen that was loaded in the fibre direction, for which there is very little total damage, even near the end of life. This sensitivity to progressive damage is greater than the authors have observed for any other method over many years of research.

3.4 Ability to capture evolving nature of damage

Another important aspect of the results is that the shape of the response curves changes as the nature of the damage changes. Damage in the early part of the life is likely to consist primarily of the initiation of micro-cracking, as suggested in Fig. 7. The EIS curves during this period (in the frequency range displayed) have a generally simple concave downward shape. Later in the life, the micro-damage grows, combines, and interacts, as shown on the right of Fig. 7. In those stages, the lower frequency imaginary component of the impedance (to the right of the figure) drops sharply in magnitude, indicating a sharp decrease in capacitive resistance.

3.5 Distinguishing directional response of heterogeneous material systems

As stated earlier, in our novel approach, the material itself acts as a sensor to represent interactive contributions of concurrent mechanisms to the material state changes. If the material has directional properties, the EIS signal should carry the possible differences in response as the material is loaded in different directions. As progressive damage develops in on-axis (warp and fill direction for woven laminate) and off-axis specimens, the EIS curves represents important features.

Whereas the 0° (warp) and 90° (fill) orientations show similar trend, the off-axis (45° orientation) presents new and different traits (Figs 10 and 11). The most obvious of those is the significant decrease in overall impedance magnitude even at 25% of life, over

https://doi.org/10.1017/S0001924000003444 Published online by Cambridge University Press

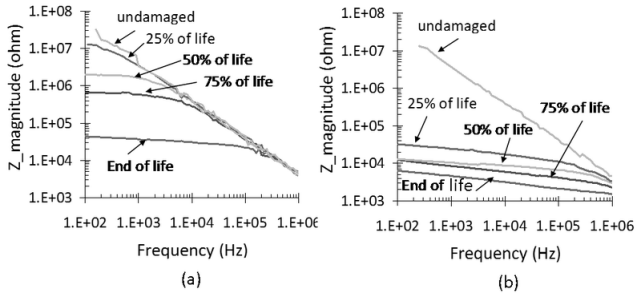


Figure 10. Bode plot of impedance magnitude *vs* frequency of excitation for several fractions of total life of (a) 0° (warp) specimen (b) 45° specimen.

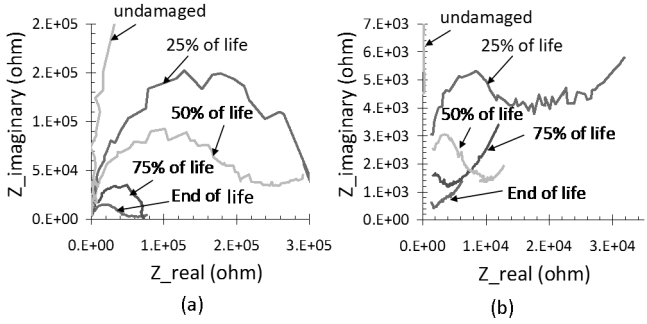


Figure 11. Nyquist plot of imaginary *vs* real part of impedance for several fractions of total life of (a) On-axis (90° or fill) specimen (b) Off-axis (45°) specimen.

two orders of magnitude lower than those observed for the on-axis cases (Fig. 10). This can be attributed to the significant increase in matrix damage experienced for off-axis specimens which creates more hydration sites.

The second notable feature is the change in AC impedance at high frequencies. For the on-axis cases, the impedance converges at high frequencies (Fig. 10(a)) and differences in the magnitude are most observable when the frequency falls below 10,000Hz. For the 45° orientation (Fig. 10(b)) however there is a constant change throughout the frequency range indicating significant changes in both capacitance as well as resistance. This new change in resistance not observed for the on-axis cases indicates that continuous conduction paths are being formed through the thickness of the specimen. Also, traditional resistance measurement (DC) approaches certainly miss such additional information.

The Nyquist plot of imaginary *vs* real part of impedance (Fig. 11) also shows important distinctive behaviours. For on-axis specimens, the imaginary part is zero when the real part is zero. But for off-axis specimens, there is a shift in this response. In addition, the downward shift of the curve for on-axis specimens (as in Fig 11(a)) is reversed after a certain point for the off-axis specimen (as in Fig 11(b)). Such features merit a closer investigation of underlying mechanism and their EIS interpretation. The key lesson here is again the ability to capture such behaviour that discriminates physical differences.

The interpretation of EIS curves is an art, and a developing science. The 'standard' method of interpretation is based on fitting the data to an analogue electrical circuit, and discussing the variation in results based on the identification of the analogue resistors, capacitors, and inductors with various general material features (and interfaces) in the general sense. However, in principle, it is possible to solve field equations of actual local geometries to associate collective impedance with specific local details of material microstructure, defects, and interfaces. That work is in progress in our laboratories, and will be discussed in a later paper.

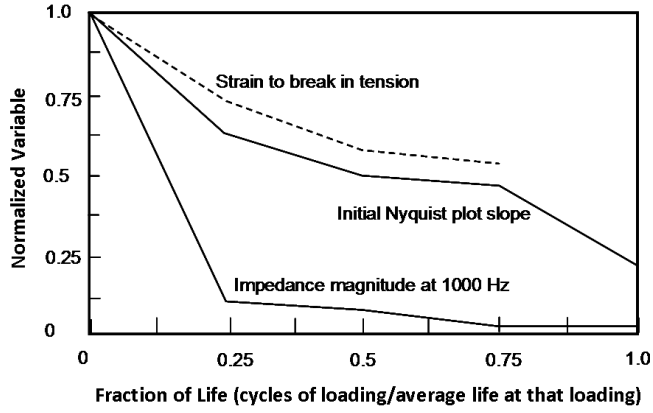


Figure 12. Comparison of normalised progressive damage accumulation as a function of the fraction of life for specimens tested[19].

3.6 Using EIS data for prognosis

For the present discussion, it will suffice to carry two conclusions from this section to our final discussion. The first conclusion is that the EIS method discussed here (with other details in Refs 18-19) is remarkably sensitive to the details of internal damage development in woven-fibre reinforced polymer composites of the type tested, and (because of it's non-invasive and multi-physics nature) could be used as a real-time monitor of those details during long-term service of composite structures. For example, some of the conductive screen skins now used to mitigate lightening strike on commercial composite airplane structures could be used (if deployed on both surfaces) for exactly these measurements.

The second conclusion is that the actual progress of the degradation in terms of life and remaining strength can be related to EIS data. Fazzino has made comparisons of different measurements of damage development including:

1. the initial slope of the EIS data shown in Fig. 9
2. the absolute value of the impedance at 1,000Hz with cycles of loading
3. damaged area determined from microscope observations and
4. remaining strain to break.

Figure 12 shows an example of such a comparison. Data were recorded at 25, 50, 75 and 100% of life, form multiple specimens; average values are shown[19].

For just the two EIS characteristics selected, there are clearly relationships between these data and fractional life; many other characteristics could have been selected in the robust EIS data set, and more research is clearly warranted here. Also, there is the question of how this method might be applied to flight structures. As it happens, moisture condensation on the interior of aircraft skins and structures is a nearly ubiquitous condition, and is a driver for the adoption of composite materials, at least in commercial aircraft. How to quantise the level of relative humidity, the conductivity of the moisture present, and the time for diffusion is a question to be addressed by sensors and additional engineering.

4.0 PROGNOSIS FOR AERONAUTICAL STRUCTURES

We close with a possible scenario for prognosis of aeronautical (composite) structures, with the reminder that many alternative approaches are possible and that much science is still to be done to support this engineering method.

https://doi.org/10.1017/S0001924000003444 Published online by Cambridge University Press

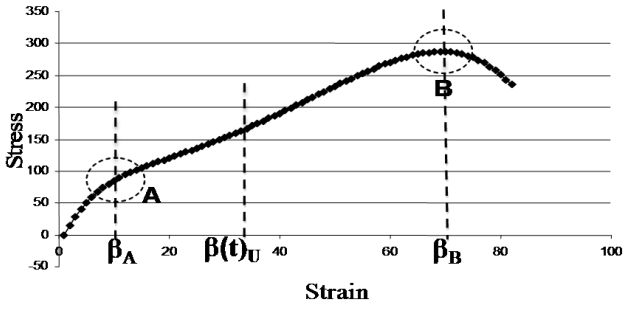


Figure 13. Generalised form of the constitutive master curve for the representation of all loading angles with transition points 'A' and 'B' indicated.

We start with the assumption that a real-time method of recovering EIS data from composite structures in service can be engineered, either a large area method based on very thin electrically conductive screens embedded into the surfaces of composite sheets, or a series of focused measurements of 'critical areas' such as joints. From this, or other methods, data such as those shown above are recorded in real time for specific structures during operation or depot testing during regular inspections.

Second, characteristics of the EIS results, such as the phenomenological ones noted in Figs 10-12 or (preferably) mechanistic ones established from further research to establish local relationships between AC conductance and micro-damage details, will provide specific information about the extent and local nature of damage as a foundation for the evaluation of remaining stiffness and strength (or strain to break) at an instant of analysis. For example, at the phenomenological level, we consider the master curve illustrated in Fig. 3 in a generalised form, as shown in Fig. 13 below.

We recall that such a master curve is attained by correctly choosing the constants in the plastic potential function, and that this single curve carries all information about the material response when loaded in all possible directions relative the material (fibre) axes. It is a simple matter to write a stress strain equation that represents the form in Fig. 13, in terms of the transition point values, *A* and *B*, as follows.

$$\sigma = \left(\left(E^e \varepsilon - \left(E^e - E^p \right) \left(1 - \exp\left(- \left(\frac{\varepsilon}{\beta_A} \right) \right) \right) \varepsilon \right) \exp\left(- \left(\frac{\varepsilon}{\beta_B} \right)^n \right) - m \qquad \ldots (12)$$

where the elastic and plastic modulus (slope) is E^e and E^p respectively, β_A and β_B are the strain values of the transition points marked in Fig. 13, n is a material constant (typically of the order 10), and m is a material constant that starts the curve out at the origin. In this form, it is clear that β_B is associated with the strain to break, and β_A is associated with the onset of plastic strain. In our deliberations above, we found that the strain to break can also be represented as a single material constant, for all loading directions (and loading rates), using the same functional form determined for the plastic potential. Then we can define the quantity $(\beta_B - \beta_A)$ as the 'available ductility', and talk about fraction of life (or strength) remaining after a given loading in terms of the ratio

$$\varepsilon^R = \frac{\left(\beta_B - \beta(t)_U \right)}{\left(\beta_B - \beta_A \right)} \qquad \ldots (13)$$

where ε^R is the ratio of the remaining ductility at an instant of measurement, t (measured by the difference between the unloading (permanent) strain, $\beta(t)_U$, and the strain to break, β_B to the 'available ductility of the material $(\beta_B - \beta_A)$, measured from the master curve for the material, Fig. 13. The unloading strain is easily determined for each point on the master curve from unloading data, as shown in Fig. 14 below.

The consistency of this concept with the physically measured unloading data are confirmed by the loading — unloading example shown in Fig. 15 below.

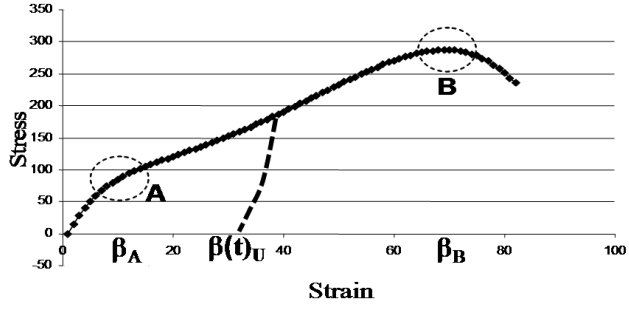


Figure 14. Example data for unloading, showing the determination of the instantaneous value of permanent strain.

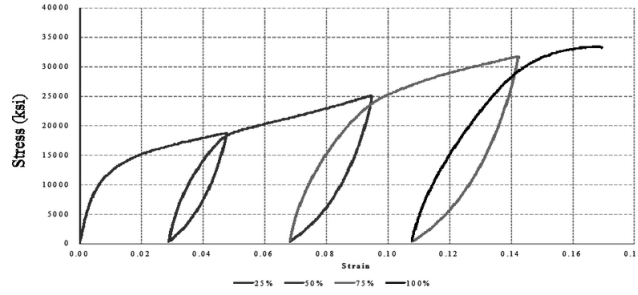


Figure 15. Example of unloading data at 25%, 50%, and 75% of the quasi-static strain to break.

With these definitions in hand we could construct a prognosis scenario in the following manner, for example:

1. EIS data are collected during the history of loading of a composite structure, either in local regions of special interest, or as field values over the structure.
2. At any point in that history, a selected characteristic of the EIS data (e.g., the initial slope of the Nyquist plot, magnitude of impedance at a specific frequency, etc. as discussed in Fig. 12) is compared to data such as that in Fig. 14 to determine how much 'available ductility' has been expended. For example, we might argue that when our electrically insulating material develops a fracture path (or a near-fracture path) for moisture ingress, we would expect the imaginary part of the impedance to drop to essentially zero, since the real (Ohmic) conductance will dominate at that point. Then we might postulate that the fraction of expended 'available ductility' at any point is equal to the fraction of expended (imaginary) impedance. That fraction will tell us where the local damage development is along the abscissa in Figs 13 and 14, and therefore, how much ductility is left (remaining strain to break).
3. For a prescribed mission to be undertaken after this evaluation point, an evolution of the EIS data as a function of the prescribed loading history must be estimated, so that a simulation of the evaluation described in (2) above can be conducted. This requires estimates of the shape of curves such as those in Figs 10-12, as a function of applied load level (in the context of a single master curve). Again, a phenomenological or mechanistic approach to those estimates can be taken. The general shape of the curves in Figs 10-12 are not complex, and with the help of some understanding of EIS data at the fundamental mechanistic level, one can imagine that evolution rates can be estimated from first principles, as suggested by Tamuzs and others[11,12].
4. If the prescribed mission is then undertaken, real-time EIS data will then provide a 'stimulation' of the simulation of degradation, to correct the estimates as the history develops, for the

https://doi.org/10.1017/S0001924000003444 Published online by Cambridge University Press

specific composite structure (e.g. airframe) for which the history was taken and for which the projected mission was specified. As the mission develops, the estimates of projected performance will become more and more accurate.

Much is yet to be done to provide the details of this sequence. In addition to the relationship between Figs 12 and 13, we have one more observation to add to the association between our fatigue data, the EIS information, and the expended ductility criterion. Figure 14 provides the basis for that.

In that figure, the total amplitude of impedance is plotted as a function of frequency for different fractions of life of a specimen. It can be seen that the contribution of the compliance (the straight line with negative slope at the beginning of life) systematically decreases until the Ohmic conductance (which is independent of frequency) dominates, indicating the development of conductive paths in the specimen. These conductive paths are micro-fracture paths, and potential fracture paths. The fraction of real conductive response verses capacitive response is also an excellent analogue of the remaining ductility fraction.

5.0 CONCLUSIONS

The present paper develops a philosophy and methodology for the prognosis of future performance of aeronautical composite structures based on history of use and current material state. The methodology is based on the general concept that local values of stiffness, strength, and conductivity (for example) are altered by material degradation to create 'property fields' that replace the global material 'constants,' and introduce time and history into the governing equations for performance and response. The methodology includes three major elements: nonlinear constitutive equations for large strains (up to and including the break strain) that support fully non-linear stress-strain analysis throughout structural life, in the presence of progressive damage; electrochemical impedance spectroscopy methods of following the local, mechanistic details of the development of damage and the consequent changes in material state, in real time, with multi-physics interpretations of the data in terms of micro-damage development and conduction path comparisons to fracture path development; and prognosis of future performance based on simulations of response based on current material state and projected state changes as a function of the projected mission. The first of these elements is well in hand. An extensive data base and a group of published work by the authors confirm that a robust progressive damage constitutive methodology has been constructed. The second element has reached the level of proof of concept. Experiments confirm that EIS data provide a remarkably sensitive and extremely robust experimental space of information that relates directly to the development and accumulation of micro-damage in the materials considered. There is every reason to believe that the physics of conductivity in the presence of fragmented conduction path development in heterogeneous materials can provide mechanistic interpretations of these data as a result of future work. For the present paper, only a phenomenological interpretation has been suggested. The third element of evolution rate equations, based on either phenomenological or mechanistic methods, is largely conjectural at this point.

However, the development of EIS as an assessment method for material state changes has opened a new door of opportunity to make the material itself the sensor, and the material state (as represented by the material constants in multi-physics equations — like the field equations for complex conductivity of heterogeneous materials) the metric for performance and prognosis. Much is yet to be done, but the results of this first effort point to many opportunities for progress.

6.0 FUTURE WORK

As we have stated, this paper is a first step towards the new concept of prognosis based on material state changes tracked using impedance spectroscopy (EIS). A number of avenues need to be addressed with greater detail in future work, such as (but not limited to):

- Quantitative assessment of the physical details that cause changes in EIS signals for various damage modes and conduction paths.
- Real-time (preferred) or intermittent (must be easy to implement) approaches for applying this methodology to large structures.
- Different alternative constitutive formulations (including partial or full unloading) covering various real life scenarios. Note that for out-of-plane loading, the concept of unloading may not be very straight forward (for example, in the plastica formulation[23], part of the structure can unload while global loading continues) and getting a closed form solution may be challenging.
- Formulation of prognosis in a way (probably in the form of a simple code) that can be conveniently used by the target audience (aerospace or other industry).

ACKNOWLEDGEMENTS

The authors gratefully acknowledge the support of the Air Force Office of Scientific Research under grant number FA9550-07-1-0460 and the Office of Naval Research under grant no. N00014-05-1-0103.

REFERENCES

1. STULL, C.J., EARLS, C.J. and WILKINS, A.P. Posteriori initial imperfection identification in shell buckling problems, *Comput Methods Appl Mech Eng*, 2008, **198**, pp 260-268.
2. HARTMANN, D., BREIDT, M., NGUYEN, V., STANGENBERG, F., HOHLER, S., SCHWEIZERHOF, K., MATTERN, S., BLANKENHORN, G., MOLLER, B. and LIEBSCHER, M. Structural collapse simulation uinder consideration of uncertainty — fundamental concept and results, *Computers and Structures*, 2008, **86**, pp 2064-2078.
3. WILLIAMS, P. Structural damage detection from transient responses using square-root unscented filtering, *ACTA Astronautica*, 2008, **63**, pp 1259-1272.
4. SU, Z.Q., YE, L. and LU, Y. Guided lamb waves for identification of damage in composite structures: a review, *J Sound and Vibration*, 2006, **295**, (3-5), pp 753-780.
5. STASZEWSKI, W.J. *ET AL*. Structural health monitoring using scanning laser vibrometry: I. lamb wave sensing, *Smart Materials and Structures*, 2004, **13**, (2), pp 251-260.
6. PAPAZIAN, J.M., ANAGNOSTOU, E.L., ENGEL, S.J., HOITSMA, D., MADSEN, J., SILBERSTEIN, R.P., WELSH, G. and WHITESIDE, J.B. A structural integrity prognosis system, *Engineering Fracture Mechanics*, 2008.
7. BIELER, T.R., EISENLOHR, P., ROTERS, F., KUMAR, D., MASON, D.E., CRIMP, M.A. and RAABE, D. The role of heterogeneous deformation on damage nucleation at grain boundaries in single phase metals, *Int J Plasticity*, 2008.
8. OGIHARA, S. and REIFSNIDER, K.L. *Applied Composite Materials*, 2002, **9**, pp 249-263.
9. REIFSNIDER, K.L., TAMUZS, V. and OGIHARA, S. *Composites Sci and Tech*, 2006, **66**, pp 2473-2478.
10. SUN C.T. and CHEN, J.L. *Composite Materials*, **23**, 1009-11020, 1989.
11. TAMUZS, V.M, DZELZITIS, K. and REIFSNIDER, K.L. *Applied Composite Materials*, 2004, **11**, (5), pp 281-293.
12. TAMUZS, V., DZELZITIS, K. and REIFSNIDER, K.L. *Applied Composite Materials*, 2004, **2**, pp 281-293.
13. REIFSNIDER, K.L and CASE, S. *Damage Tolerance and Durability of Material Systems*, 2002, John Wiley & Sons, New York, USA.

https://doi.org/10.1017/S0001924000003444 Published online by Cambridge University Press

14. XING, L. Progressive Failure of Large Deformation Woven Composites under Dynamic Loading, 2007, PhD dissertation, Department of Mechanical Engineering, College of Engineering, University of Connecticut, USA.
15. REIFSNIDER,K. and XING, L. Large-deformation constitutive theories for structural composites: rate-dependent concepts and effect of microstructure, *Strain*, 2007, **44**, (1), pp 119-125.
16. MONKMANN, F.C. and GRANT, N.S. *Proceedings American Society of Test Materials*, 1956, **56**, pp 593-620.
17. HUFFNER, D. Progressive Failure of Woven Polymer-Based Composites under Dynamic Loading; Theory and Analytical Simulation, 2008, Dissertation, Department of Civil and Environmental Engineering, University of Connecticut, USA.
18. FAZZINO, P. Predictive Methods for Large-scale Progressive Damage in Structural Composites for Aircraft Applications, November 2008, Masters thesis, Department of Mechanical Engineering, College of Engineering and Computing, University of South Carolina, USA.
19. FAZZINO, P. and REIFSNIDER, K.L. Electrochemical impedance spectroscopy detection of damage in out of plane fatigued fiber reinforced composite materials, *Applied Composite Materials*, 2008, **15**, (3), pp 127-138.
20. LASIA, A. Electrochemical impedance spectroscopy and its applications, *Modern Aspects of Electrochemistry*, 1999, **32**, pp 143-248, CONWAY, B.E., BOCKRIS, J. and WHITE, R.E. (Eds), Kluwer Academic/Plenum Publishers, New York, USA.
21. FAZZINO, P., REIFSNIDER, K. and MAJUMDAR, P. Impedance spectroscopy of fabric reinforced composites, 2009, Proceedings of SAMPE 2009 Conference, 18-21 May 2009, Baltimore, MD.
22. BAMFORD, D.J. Progressive Damage and Delamination in Composite Plates under Dynamic Loading: Analytical Modeling and Experimental Validation, PhD dissertation, 2008, University of Connecticut, USA.
23. MAJUMDAR, P, FAZZINO, P. and REIFSNIDER, K. Behavior of woven fabric composites in off-axis end-loaded bending, 2009, SAMPE 2009 Conference Proceedings, 18-21 May 2009, Baltimore, MD, USA.

https://doi.org/10.1017/S0001924000003444 Published online by Cambridge University Press